International Journal of
MATERIALS RESEARCH

Zeitschrift für METALLKUNDE

Original Contributions

Yuxun Jiang[a], Setareh Zomorodpoosh[b], Irina Roslyakova[b], Lijun Zhang[a]
[a] State Key Laboratory of Powder Metallurgy, Central South University, Changsha, Hunan, P.R. China
[b] ICAMS, Ruhr-Universität Bochum, Universitätsstrasse 150, Bochum, Germany

Thermodynamic re-assessment of the binary Cr–Ta system down to 0 K

On the basis of the recently proposed physically-based segmented model, the descriptions for the Gibbs energy of pure Cr and Ta down to 0 K were first established. After that, a thermodynamic re-assessment of the binary Cr–Ta system down to 0 K was then performed by taking into account all the critically reviewed experimental phase equilibria and thermodynamic properties. Especially, the experimental heat capacities of Cr_2Ta at low temperatures ignored in previous assessments were utilized in the present assessment. The calculated phase equilibria and thermodynamic properties according to the presently obtained thermodynamic descriptions of the binary Cr–Ta system agree well with most of the experimental data, and show better agreement than the previous assessment.

Keywords: Cr–Ta; Thermodynamics; CALPHAD; Heat capacity; 0 K

1. Introduction

Cr–Ta alloys strengthened by the Cr_2Ta Laves phase possess high melting points and good strength at elevated temperatures, and thus serve as promising candidates for high temperature structural applications [1–7]. The CALculation of PHAse Diagram (CALPHAD) approach has been proved to be a powerful tool in guiding the design of novel alloys in recent years [8, 9], but a high-quality thermodynamic database for the target systems is a prerequisite. Consequently, an accurate CALPHAD thermodynamic description of the binary Cr–Ta system is a necessity for material developments concerning Cr and Ta additions.

There are already several sets of thermodynamic descriptions for the binary Cr–Ta system in the literature. Kaufman [10] performed a thermodynamic calculation for the binary Cr–Ta system as early as in 1991. However, in Ref. [10] the intermetallic phases in the types of Laves_C14 and Laves_C15 were treated as stoichiometric phases, and the predicted solubility of terminal solid solution shows large discrepancies with the experimental data. Later in 1993, Dupin and Ansara [11] re-assessed this system, and their calculated results can reproduce most of the experimental data available in the literature. Nevertheless, due to the unlimited usage of interaction parameters of the Laves phases, an unexpected miscibility gap appears at relatively high temperatures according to the thermodynamic parameters published in Ref. [11]. The problem was spotted by Zhang et al. [12], who performed another thermodynamic assessment for the Cr–Ta system by introducing composition-independent interaction parameters. Very recently, Pavlů et al. [13] performed a re-modeling of the Laves phase by applying their own first-principles results. However, both of the two latter assessments [12, 13] focused on the re-modeling on thermodynamic description of Laves_C15 phase and kept the same thermodynamic parameters for liquid and bcc phases as those in Ref. [11].

Very recently, the 3rd generation thermodynamic database has gained great interest among the CALPHAD community. Several new thermodynamic models applying physical meaning have been proposed for better extrapolations and predictabilities of thermodynamic properties of materials [14–18]. Another important aspect for developing the 3rd generation thermodynamic database is the ex-

pectation of obtaining reliable and accurate thermodynamic descriptions from 0 K to high temperatures above the melting points [19]. Aiming at the objectives mentioned above, Roslyakova et al. proposed a new strategy in modeling the thermodynamic descriptions for pure elements down to 0 K by combining the physically based segmented model [20] and approximation method of the Debye model [21]. In our very recent work on thermodynamic re-assessment of Cr–Nb down to 0 K [22], the Gibbs energies for unary Cr and Nb were modeled through method suggested by Roslyakova et al. Besides, using the same approach, the thermodynamic descriptions for heat capacities of stoichiometric compound Cr_2Nb ignored in previous thermodynamic assessments were also able to be well established. Similarly, in the case of thermodynamic assessments of Cr–Ta, the heat capacities of stoichiometric compound Cr_2Ta were also ignored in the previous assessments [10–13]. However, the heat capacity data are of great importance for obtaining the high-quality thermodynamic descriptions for binary Cr–Ta system using the CALPHAD approach.

Consequently, a re-assessment of the binary Cr–Ta system down to 0 K is performed in the present work. The thermodynamic descriptions for pure elements and stoichiometric compound Cr_2Ta are conducted by applying the extended segmented model developed by Roslyakova et al. [21]. Moreover, the heat capacities measured at low temperatures [23] missing in all previous assessments are utilized in the current thermodynamic assessment.

2. Literature review

The binary Cr–Ta system comprises three solid phases aside from the liquid phase: the BCC_A2 based (Cr) and (Ta) solid solutions, and two intermetallic phases in types of low-temperature Laves_C15 and high-temperature Laves_C14. All the experimental phase equilibria and thermodynamic properties of the binary Cr–Ta system available in literature are summarized in Table 1 and concisely categorized in the following.

2.1. Phase equilibria information

The liquidus and solidus were first studied by Kubaschewski and Speidel [24] using thermal analysis in 1949. About ten years later, Grigorev et al. [25] reported the liquidus around Laves_C14 phase with the same method. However, the liquidus and solidus of Cr–Ta system cannot be deli-

Table 1. Summary of the phase diagram and thermodynamic data in the Cr–Ta system available in the literature.

Type of data	Reference	Experimental method	Quoted mode[a]
Liquidus			
0–100 at.% Ta	[26]	TA	–
0–100 at.% Ta	[24]	TA	–
0–77 at.% Ta	[25]	TA	–
Solidus in Cr-rich part	[24]	TA	–
Solidus in Ta-rich part	[26]	TA	+
Cr-solvus	[33]	XRD	+
Ta-solvus	[34]	XRD	+
Congruent melting point	[27]	DTA	–
	[25]	TA	–
	[26]	DTA	–
	[28]	DTA	–
	[29]	Assessed	+
Eutectic in Cr-rich part	[24]	TA	–
	[25]	TA	–
	[26]	TA	+
	[28]	DTA	–
	[29]	Assessed	–
Eutectic in Ta-rich part	[25]	TA	–
	[26]	TA	+
	[28]	DTA	–
	[29]	Assessed	–
Eutectoid & Peritectoid	[26]	DTA	+
Enthalpy of formation of Laves_C15 at 1693 K	[32]	Adiabatic calorimeter	+
Activities of Cr at 1472 K	[32]	Knudsen cell effusion	+
Heat capacities of Cr_2Ta	[23]	Adiabatic calorimetry	+

TA = Thermal analysis.
DTA = Differential thermal analysis.
XRD = X-ray diffraction.
[a] indicates whether the data are used or not used in the parameter optimization: + used; − not used but employed for comparison

neated thoroughly based on their results [24, 25]. The investigation of liquidus and solidus over the whole composition range were executed by Rudy [26] using differential thermal analysis (DTA) and thermal analysis (TA). However, the results due to Rudy [26] are inconsistent with the earlier two groups of data [24, 25]. Though the experimental data from Rudy [26] are preferred, it should also be noted that the liquidus data were recorded at the time when the specimen collapsed, which introduces relatively large error into the results. Besides, the solidus of (Ta) was not detected clearly by Rudy [26] either. Thus, among the experimental data mentioned above, only the solidus data for (Cr) and Laves_C14 reported by Rudy [26] are considered in the present thermodynamic assessment.

According to the existing investigations [25–28], the high-temperature Laves_C14 phase melts congruently. What is more, the congruent melting temperatures from different sources are in good agreement with each other, and a value of 2293 ± 20 K was proposed in the assessed phase diagram by Venkatraman and Neumann [29], which was also accepted in the previous thermodynamic assessments [11–13]. Thus, the same value is also included in the optimization procedure of the present work. The eutectic reaction in Cr-rich part, L ↔ (Cr) + Laves_C14, was measured by different sources [24–26, 28]. However, the temperature provided by Kubaschewski and Speidel [24] and Grigorev et al. [25] is lower than that from Rudy [26] and Kocherzhinskii et al. [28] by several tens of degrees Celsius. Besides, recent studies by Brady et al. [2, 6, 30] indicate that the composition of this reaction should be 9.7 at.% Ta, which is in general agreement with value of 10.5 at.% Ta by Rudy [26], but not with the assessed value by Venkatraman and Neumann [29]. The value of 13 at.% Ta adopted by Venkatraman and Neumann [29], which was also accepted in the previous assessments [11–13], is regarded to have a large error. While for the other eutectic in Ta-rich part, L ↔ (Ta) + Laves_C15, was studied by [25, 26, 28]. Their results are in general agreement with each other taking the experimental uncertainties into consideration. As for the invariant reactions during the solid state phase transformation (i.e. eutectoid and peritectoid), the measurements by Rudy [26] using DTA give reliable composition and temperatures rather than ambiguous ranges by other authors [25, 28, 31, 32], and thus these results [26] are adopted here. Hence, in the present optimization, the compositions and temperatures of the invariant reactions are all derived from Rudy's [26] measurements except the data for congruent melting, which was kept as the same with the previous assessments [11–13, 29].

The solubilities of Cr in (Ta) and Ta in (Cr) were measured by Auld and Ryan [33] and Gebhardt and Rexer [34] using X-ray diffraction (XRD) respectively. They are very impotant for construction of the Cr–Ta phase digram and will also be utilized in the present work.

Table 2. Gibbs energy for pure elements[a].

Symbols	Thermodynamic parameters	Temperature range
G_{Cr}^{Liquid}	$12.43857\ T\ln(e^{280.8869/T}-1)+12.48347\ T\ln(e^{457.8066/T}-1)+11082.43989$	
	$-11.26666\cdot T-0.0034\ T^2+8.40882\times10^{-7}\ T^3$	$(0.01 < T < 298.15)$
	$15\,483.0135147752+146.059775\ T-26.908\ T\ln(T)+0.00189435\ T^2-1.47721\times10^{-6}\ T^3$	
	$+139\,250\ T^{-1}+2.37615\times10^{-21}\cdot T^7$	$(298.15 < T < 2\,186.7)$
	$-16\,459.98454+335.616316\ T-50\ T\ln(T)$	$(2\,186.7 < T < 6\,000.0)$
[b] $G_{Cr}^{BCC\_A2}$	$-13\,239.49633-0.0026915\ T^2+12.43857\ T\ln(e^{280.8869/T}-1)+12.48347\ T\ln(e^{457.8066/T}-1)+G^{mag}$	$(0.01 < T < 675.1)$
	$-14\,523.81882+34.32834\ T+0.00576243\ T^2-2.08708\times10^{-6}\ T^3-5.70725\ T\ln(T)$	
	$+12.43857\ T\ln(e^{280.8869/T}-1)+12.48347\ T\ln(e^{457.8066/T}-1)+G^{mag}$	$(675.1 < T < 1\,452.9)$
	$-1\,721.845-144.9288\cdot T-0.0124315\ T^2+20.72672\cdot T\cdot\ln(T)+12.43857\cdot T\cdot\ln(e^{280.8869/T}-1)$	
	$+12.48347\cdot T\cdot\ln(e^{457.8066/T}-1)+G^{mag}$	$(1\,452.9 < T < 2\,186.7)$
	$-35\,632.82689+344.47868\ T-50\ T\ln(T)-2.36115\times10^{32}\ T^{-9}$	$(2\,186.7 < T < 6\,000.0)$
G_{Ta}^{Liquid}	$+19\,151.8-7.02870\ T-0.00381\ T^2+2.28183\times10^{-6}\ T^3$	
	$+5.57354\ T\ln(e^{89.16941/T}-1)+19.39290\ T\ln(e^{194.28406/T}-1)$	$(0.01 < T < 298.15)$
	$+21\,875.1+111.56113\ T-23.75926\ T\ln(T)-0.00262\ T^2$	
	$+1.70109\times10^{-7}\ T^3-3\,293.0\cdot T^{-1}$	$(298.15 < T < 1\,000.0)$
	$+43\,884.3-61.98180\ T+0.02795\ T\ln(T)-0.01233\ T^2$	
	$+6.14599\times10^{-7}\ T^3-3\,523\,338.0\cdot T^{-1}$	$(1\,000.0 < T < 3\,285.9)$
	$-6\,314.5+258.11087\ T-41.84000\ T\ln(T)$	$(3\,285.9 < T < 6\,000.0)$
$G_{Ta}^{BCC\_A2}$	$-9\,930.0-0.00156\ T^2+5.57354\ T\ln(e^{89.16941/T}-1)+19.39290\ T\ln(e^{194.28406/T}-1)$	$(0.01 < T < 2\,239.9)$
	$-70\,507.0+585.31196\ T+0.03466\ T^2-2.69520\times10^{-6}\ T^3-81.13347\ T\ln(T)$	
	$+5.57354\ T\ln(e^{89.16941/T}-1)+19.39290\ T\ln(e^{194.28406/T}-1)$	$(2\,239.9 < T < 3\,285.9)$
	$-1\,011\,359.9+2\,980.30611\ T-362.1591318\ T\ln(T)+0.04313\ T^2$	
	$-1.05515\times10^{-6}\ T^3+508\,367\,455.07867\ T^{-1}$	$(3\,285.9 < T < 6\,000.0)$
T_c	+311.5	$(0.01 < T < 6\,000.0)$
β	+0.008	$(0.01 < T < 6\,000.0)$

[a] Gibbs energy in J/mol-atom; Temperature in Kelvin.
[b] The magnetic contribution to the Gibbs energy G^{mag} is described by the Hillert–Jarl–Inden model [36]

2.2. Thermodynamic information

Experimental data on the thermodynamic properties of the binary Cr–Ta system are scarce. By using an adiabatic calorimeter, Feschotte and Kubaschewski [32] studied the enthalpy of formation of Laves_C15 at 1673 K. The same authors also determined the activities in the two-phase regions of (Cr) + Laves_C15 and (Ta) + Laves_C15 at 1472 K by means of Knudsen cell effusion using a radioactive tracer (^{51}Cr). However, the activities of Cr in (Cr) + Laves_C15 show a pronounced scatter of the mean value, and a value of 0.96 was suggested by Feschotte and Kubaschewski [32] on the combination of Raoult's law as well as solubility data from Auld and Ryan [33]. The activities of Cr in (Ta) + Laves_C15 region are comparable with each other. Thus, in the present work, the suggested values of activities of Cr in (Cr) + Laves_C15 region and the measured activities of Cr in (Ta) + Laves_C15 region are introduced in the present optimization procedure. Later in 1970, Martin et al. [23] measured the heat capacities of the compound Cr_2Ta between 10 and 350 K also using an adiabatic calorimeter. These data are used in the present optimization. Furthermore, the first-principles calculations of enthalpy of formation of Cr_2Ta made by Pavlů et al. [13] will also be considered as an important parallel in the present work for validation of the obtained thermodynamic descriptions.

3. Thermodynamic model

3.1. Pure Cr and Ta

According to Roslyakova et al. [20], the heat capacities of pure elements could derive accurate descriptions for their Gibbs energy directly, in a way of considering the decomposition of several physical contributions to the heat capacities into low and high temperatures regimes. What is more, an approximation of the Debye model through the weighted linear combination of the Einstein functions was also introduced. Such strategy maintains the superiority of the Debye model in describing the temperature dependence of heat capacities at low temperature range, and makes it possible to implement the Debye model into the existing thermodynamic databases. In the present work, the same method is executed, and the obtained description of the Gibbs energy for pure Cr and Ta for the liquid phase and stable solid BCC_A2 phase are listed in Table 2

3.2. Solution phases

The liquid and BCC_A2 (i. e., (Cr) and (Ta)) phases are described as the disordered solutions. Their general molar Gibbs energy consists of the following four parts:

$$G^{\varphi} - H^{\mathrm{SER}} = G^{\mathrm{ref}} + \Delta G^{\mathrm{ideal}}_{\mathrm{mix}} + G^{\mathrm{excess}} + G^{\mathrm{mag}} \quad (1)$$

where φ denotes the phase (i.e, liquid or BCC_A2 phase). $H^{\mathrm{SER}} = x_{\mathrm{Cr}} \cdot H^{\mathrm{SER}}_{\mathrm{Cr}} + x_{\mathrm{Ta}} \cdot H^{\mathrm{SER}}_{\mathrm{Ta}}$ is the enthalpy at reference state (298.15 K, 1 bar), in the following abbreviation "SER", and $H^{\mathrm{SER}}_{\mathrm{Cr}}$, $H^{\mathrm{SER}}_{\mathrm{Ta}}$ are the molar enthalpies of pure Cr and Ta respectively. The first term of the right side of equation (1), represents the contribution from mechanical mixing of the pure elements and $\Delta G^{\mathrm{ideal}}_{\mathrm{mix}} = R \cdot T \cdot [x_{\mathrm{Cr}} \cdot \ln x_{\mathrm{Cr}} + x_{\mathrm{Ta}} \cdot \ln x_{\mathrm{Ta}}]$ denotes the ideal entropy of mixing. Assuming the role for the excess Gibbs energy in form of the classic Redlich–Kister (R–K) polynomial [35], the third term, G^{excess}, equals to $x_{\mathrm{Cr}} \cdot x_{\mathrm{Ta}} \cdot \sum_{i=0}^{n} L^{i,\varphi}_{\mathrm{Cr,Ta}} (x_{\mathrm{Cr}} - x_{\mathrm{Ta}})^i$, where $L^{i,\varphi}_{\mathrm{Cr,Ta}}$ is the i th R–K parameters in the expression of $L^{i,\mathrm{liq}}_{\mathrm{Cr,Ta}} = a_i + b_i \cdot T$. Here a_i, b_i are the interaction parameters to be optimized in the present work. The last term of equation (1), G^{mag} is the magnetic contribution. For liquid phase, G^{mag} equals 0, while for BCC_A2 phase, it can be expressed by the Hillert–Jarl–Inden model [36]:

$$G^{\mathrm{mag}} = RT \ln(\beta^{\varphi} + 1) g(\tau^{\varphi}) \quad (2)$$

where $\tau = T/T^*$, and T^* is the Curie temperature T_{C} for ferromagnetic materials or the Neel temperature T_{N} for antiferromagnetic materials, β is the average magnetic momentum per atom. The function $g(\tau^{\varphi})$ has the polynomial representation derived from Hillert and Jarl [36], and one can refer for more details to their original paper.

3.3. Laves phases

In light of the reported homogeneity ranges, the Laves_C14 and the Laves_C15 phases are described with a two-sublattice model, $(\mathbf{Cr}, \mathrm{Ta})_2(\mathrm{Cr}, \mathbf{Ta})_1$, where the first sublattice is mainly occupied by Cr, the second by Ta and the ratio of number of sites in each sublattice is 2 : 1. Generally, the mo-

Table 3. Gibbs energy for stoichiometric coumpound Cr_2Ta[a].

Symbols	Thermodynamic parameters	Temperature range
$G^{\mathrm{Laves\_C15}}_{\mathrm{Cr_2Ta}}$	$-11\,861.1 - 0.00085 \cdot T^2 + 7.78660 \cdot T \cdot \ln(e^{152.0489/T} - 1) + 17.32440 \cdot T \cdot \ln(e^{350.7481/T} - 1)$	$(0.01 < T < 150)$
	$-11\,900.88532 + 3.58783\,T + 0.00446\,T^2 - 5.90278 \times 10^{-6}\,T^3 - 0.79556\,T \ln(T)$	
	$+7.78660\,T \ln(e^{152.0489/T} - 1) + 17.32440\,T \ln(e^{350.7481/T} - 1)$	$(150 < T < 240)$
	$-11\,737.71574 - 6.57129\,T - 0.00404\,T^2 + 1.24419 \cdot T \ln(T)$	
	$+7.78660\,T \ln(e^{152.0489/T} - 1) + 17.32440\,T \ln(e^{350.7481/T} - 1)$	$(240 < T < 4\,000)$

[a] Gibbs energy in J/mol-atom; Temperature in Kelvin.

lar Gibbs energy per formula of Laves_C15 can be expressed as follows:

$$
\begin{aligned}
{}^{0}G^{\text{Laves\_C15}} = {} & {}^{0}G^{\text{Laves\_C15}}_{\text{Cr:Ta}}\, y'_{\text{Cr}} y''_{\text{Ta}} + {}^{0}G^{\text{Laves\_C15}}_{\text{Cr:Cr}}\, y'_{\text{Cr}} y''_{\text{Cr}} \\
& + {}^{0}G^{\text{Laves\_C15}}_{\text{Ta:Ta}}\, y'_{\text{Ta}} y''_{\text{Ta}} + {}^{0}G^{\text{Laves\_C15}}_{\text{Ta:Cr}}\, y'_{\text{Ta}} y''_{\text{Cr}} \\
& + 2RT\left(y'_{\text{Cr}} \ln y'_{\text{Cr}} + y'_{\text{Ta}} \ln y'_{\text{Ta}}\right) \\
& + RT\left(y''_{\text{Cr}} \ln y''_{\text{Cr}} + y''_{\text{Ta}} \ln y''_{\text{Ta}}\right) \\
& + y'_{\text{Cr}} y''_{\text{Cr}} y''_{\text{Ta}}\, {}^{0}L^{\text{Laves\_C15}}_{\text{Cr:Cr,Ta}} + y'_{\text{Ta}} y''_{\text{Cr}} y''_{\text{Ta}}\, {}^{0}L^{\text{Laves\_C15}}_{\text{Ta:Cr,Ta}} \\
& + y'_{\text{Cr}} y'_{\text{Tay}} y''_{\text{Cr}}\, {}^{0}L^{\text{Laves\_C15}}_{\text{Cr,Ta:Cr}} + y'_{\text{Cr}} y'_{\text{Ta}} y''_{\text{Ta}}\, {}^{0}L^{\text{Laves\_C15}}_{\text{Cr,Ta:Ta}} \\
& + \cdots
\end{aligned}
\tag{3}
$$

where the superscripts $'$ denote the first sublattice and $''$ the second, y_i' and y_i'' denote the site fraction in the first and second sublattice of element i, respectively. ${}^{0}G^{\text{Laves\_C15}}_{\text{Cr:Ta}}$ is the Gibbs energy of the ideal stoichiometric compound Cr_2Ta. One important aspect in the present work is the full usage of the existing heat capacity data on stoichiometric Cr_2Ta composition at low temperature range [23]. Thus Gibbs energy for the stoichiometric compound Cr_2Ta, $G^{\text{Laves\_C15}}_{\text{Cr}_2\text{Ta}}$, can be derived from a similar approach proposed by Roslyakova et al. [20], which is listed in Table 3. Then the thermodynamic parameter, ${}^{0}G^{\text{Laves\_C15}}_{\text{Cr:Ta}}$, can be derived through the optimizing process by taking experimental data

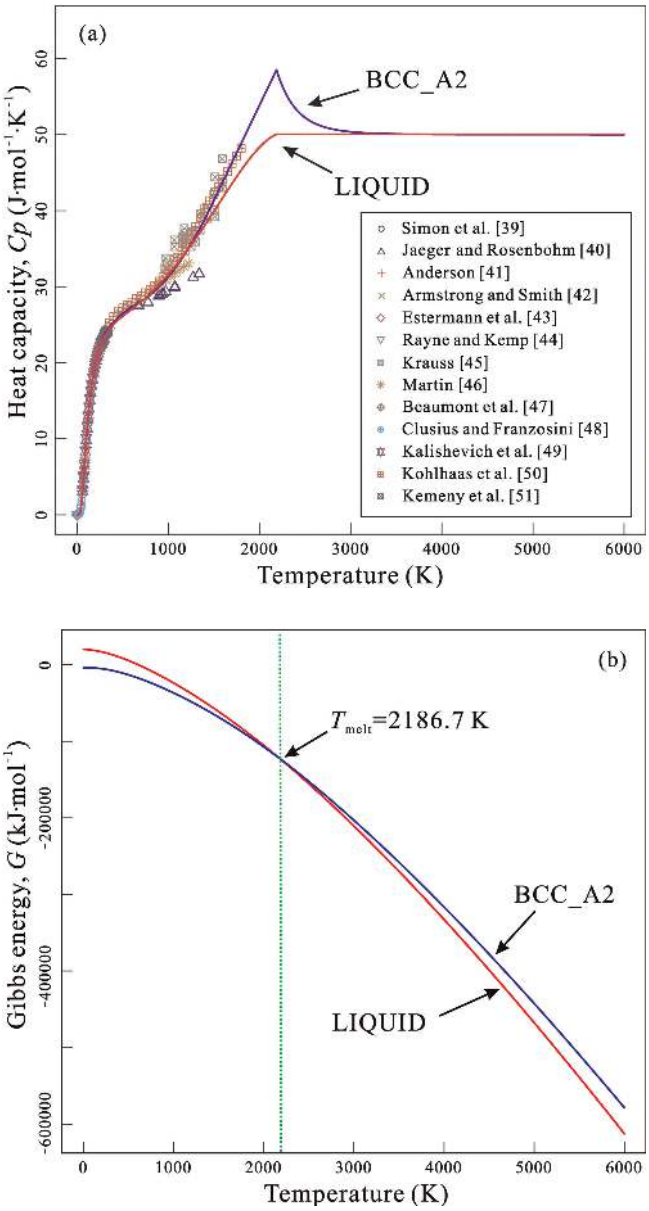

Fig. 1. (a) Fitted heat capacity of pure Cr in comparison with the experimental data from different sources, shown as points: Simon et al. [39], Jaeger and Rosenbohm [40], Anderson [41], Armstrong and Smith [42], Estermann et al. [43], Rayne and Kemp [44], Krauss [45], Martin [46], Beaumont et al. [47], Clusius and Franzosini [48], Kalishevich et al. [49], Kohlhaas et al. [50], Kemeny et al. [51]; (b) Calculated Gibbs energies of BCC_A2 and LIQUID phases for pure Cr.

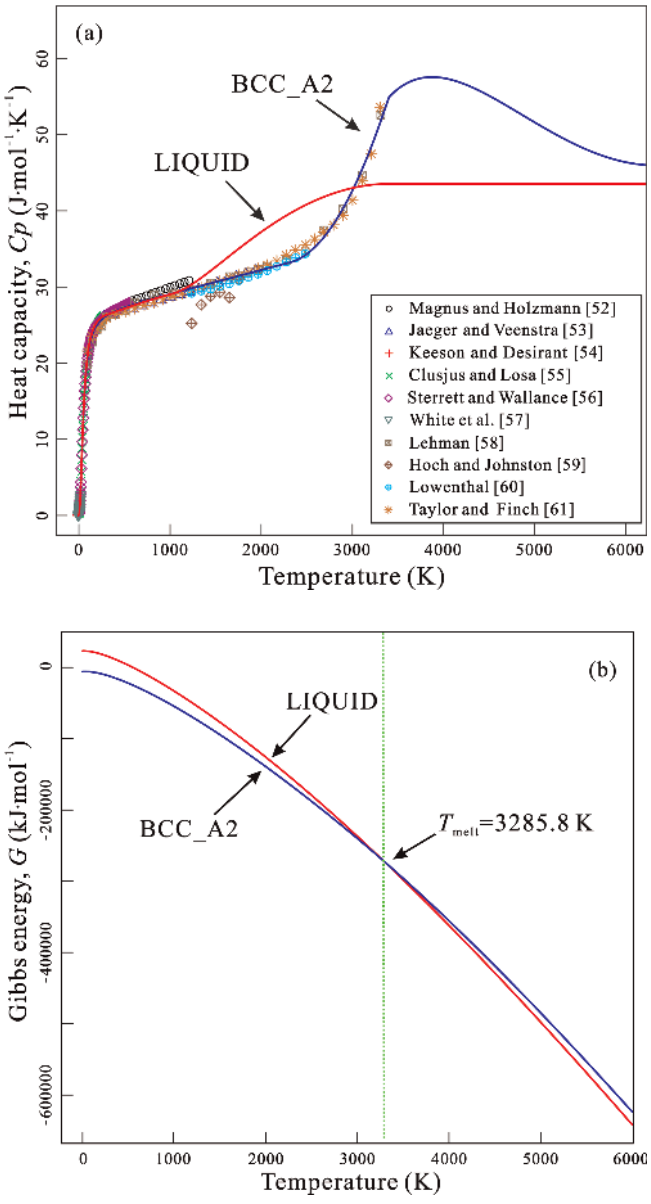

Fig. 2. (a) Fitted heat capacity of pure Ta in comparison with the experimental data from different sources, shown as points: Magnus and Holzmann [52], Jaeger and Veenstra [53], Keeson and Desirant [54], Clusjus and Losa [55], Sterrett and Wallance [56], White et al. [57], Lehman [58], Hoch and Johnston [59], Lowenthal [60], Taylor and Finch [61]; (b) Calculated Gibbs energies of BCC_A2 and LIQUID phases for pure Ta.

[23] into account. ${}^{0}G^{\text{Laves\_C15}}_{\text{Ta:Cr}}$ is the Gibbs energy for the fictitious compound $CrTa_2$. ${}^{0}G^{\text{Laves\_C15}}_{\text{Cr:Cr}}$ and ${}^{0}G^{\text{Laves\_C15}}_{\text{Ta:Ta}}$ are the Gibbs energies for fictitious pure Cr and Ta in Laves_C15 phase state. Moreover, the reciprocal relation ${}^{0}G^{\text{Laves\_C15}}_{\text{Cr:Cr}}+{}^{0}G^{\text{Laves\_C15}}_{\text{Ta:Ta}}+{}^{0}G^{\text{Laves\_C15}}_{\text{Cr:Ta}}={}^{0}G^{\text{Laves\_C15}}_{\text{Ta:Cr}}$ was applied to evaluate the parameter corresponding to ${}^{0}G^{\text{Laves\_C15}}_{\text{Ta:Cr}}$. The high temperature modification Laves_C14 phase is modeled in a similar way to that of Laves_C15 phase. The only difference lies in the description of ${}^{0}G^{\text{Laves\_C14}}_{\text{Cr:Ta}}$ since there are no experimental data available on heat capacities of the ideal stoichiometric compound Cr_2Ta at high temperature, thus it is expressed by an equation of ${}^{0}G^{\text{Laves\_C14}}_{\text{Cr:Ta}} = {}^{0}G^{\text{Laves\_C15}}_{\text{Cr:Ta}} + A_0 + B_0 \cdot T$. Here, A_0 and B_0 are two parameters to be assessed in the present work.

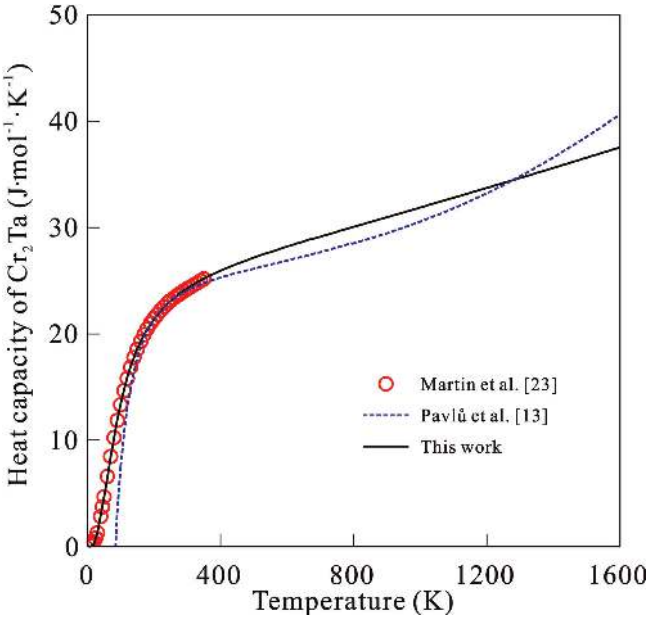

Fig. 3. Calculated heat capacities of the Laves_C15 phase at the stoichiometric composition compound, compared with the calculated results by Pavlů et al. [13], and the experimental data from Martin et al. [23].

The second part of (3), i.e., $2 \cdot RT \cdot \left(y'_{\text{Cr}}\ln y'_{\text{Cr}} + y'_{\text{Ta}}\ln y'_{\text{Ta}}\right) + RT \cdot \left(y''_{\text{Cr}}\ln y''_{\text{Cr}} + y''_{\text{Ta}}\ln y''_{\text{Ta}}\right)$, means the contribution from ideal entropy of mixing. L s are the interaction parameters as mentioned above. Furthermore, ${}^{0}L^{\text{Laves}}_{\text{Cr:Cr,Ta}} = {}^{0}L^{\text{Laves}}_{\text{Ta:Cr,Ta}} = {}^{0}L^{\text{Laves}}_{*\text{:Cr,Ta}}$ and ${}^{0}L^{\text{Laves}}_{\text{Cr,Ta:Cr}} = {}^{0}L^{\text{Laves}}_{\text{Cr,Ta:Ta}} = {}^{0}L^{\text{Laves}}_{\text{Cr,Ta:}*}$ are engaged in the present optimization for both Laves_C14 and Laves_C15 phase based on the assumption that interaction between two species in one sublattice is independent of occupation in the other sublattice.

4. Results and discussion

The Gibbs energies for pure elements and the stoichiometric compound Cr_2Ta were modeled using the same method as illustrated in our previous Cr–Nb system [22]. The fitted heat capacities for BCC_A2 of pure Cr and Ta in comparison with the considered experimental data sets are shown in Figs. 1a and 2a [39–61], respectively. In both cases, one can observe a good agreement between the calculated results and the experiments. The heat capacities of the Laves_C15 phase at the stoichiometric composition Cr_2Ta were calculated, and compared with the calculated results obtained in the previous assessments [13] and the experi-

Table 4. Summary of the finally obtained thermodynamic parameters in the Cr–Ta system[a].

Symbols	Thermodynamic parameters	Temperature range
Liquid: $(Cr,Ta)_1$		
${}^{0}L^{\text{Liq}}_{\text{Cr:Ta}}$	+42 575.0 – 24.5884 T	$(0.01 < T < 6000.0)$
${}^{1}L^{\text{Liq}}_{\text{Cr:Ta}}$	+43 721.0 – 18.2472 T	$(0.01 < T < 6000.0)$
${}^{2}L^{\text{Liq}}_{\text{Cr:Ta}}$	–27 084.6 + 6.3146 T	$(0.01 < T < 6000.0)$
BCC_A2: $(Cr,Ta)_1(Va)_3$		
${}^{0}L^{\text{BCC\_A2}}_{\text{Cr:Ta}}$	+93 845.5 – 35.5118 T	$(0.01 < T < 6000.0)$
${}^{1}L^{\text{BCC\_A2}}_{\text{Cr:Ta}}$	+53 672.3 – 23.8329 T	$(0.01 < T < 6000.0)$
${}^{2}L^{\text{BCC\_A2}}_{\text{Cr:Ta}}$	–4 650.5	$(0.01 < T < 6000.0)$
Laves_C15: $(Cr,Ta)_2(Cr,Ta)_1$		
${}^{0}G^{\text{Laves\_C15}}_{\text{Cr:Ta}}$	–26 780 – 0.1026 T + 3 $G^{\text{Laves\_C15}}_{\text{Cr}_2\text{Ta}}$	$(0.01 < T < 6000.0)$
${}^{0}G^{\text{Laves\_C15}}_{\text{Cr:Cr}}$	+55 347.2 + 3 $G^{\text{BCC\_A2}}_{\text{Cr}}$	$(0.01 < T < 6000.0)$
${}^{0}G^{\text{Laves\_C15}}_{\text{Ta:Ta}}$	+43 219.5 + 3 · $G^{\text{BCC\_A2}}_{\text{Ta}}$	$(0.01 < T < 6000.0)$
${}^{0}G^{\text{Laves\_C15}}_{\text{Ta:Cr}}$	${}^{0}G^{\text{Laves\_C15}}_{\text{Cr:Cr}}$ + ${}^{0}G^{\text{Laves\_C15}}_{\text{Ta:Ta}}$ – ${}^{0}G^{\text{Laves\_C15}}_{\text{Cr:Ta}}$	$(0.01 < T < 6000.0)$
${}^{0}L^{\text{Laves\_C15}}_{\text{Cr,Ta:}*}$	+31 233.9 + 12.0000 T	$(0.01 < T < 6000.0)$
${}^{0}L^{\text{Laves\_C15}}_{*\text{:Cr,Ta}}$	–4 603.0 + 1.0004 T	$(0.01 < T < 6000.0)$
Laves_C14: $(Cr,Ta)_2(Cr,Ta)_1$		
${}^{0}G^{\text{Laves\_C14}}_{\text{Cr:Ta}}$	+8 834.1 – 18.2469 T + 3 $G^{\text{Laves\_C15}}_{\text{Cr}_2\text{Ta}}$	$(0.01 < T < 6000.0)$
${}^{0}G^{\text{Laves\_C14}}_{\text{Cr:Cr}}$	+57 693.9 + 3 · $G^{\text{BCC\_A2}}_{\text{Cr}}$	$(0.01 < T < 6000.0)$
${}^{0}G^{\text{Laves\_C14}}_{\text{Ta:Ta}}$	+3 286.6 + 3 · $G^{\text{BCC\_A2}}_{\text{Ta}}$	$(0.01 < T < 6000.0)$
${}^{0}G^{\text{Laves\_C14}}_{\text{Ta:Cr}}$	${}^{0}G^{\text{Laves\_C14}}_{\text{Cr:Cr}}$ + ${}^{0}G^{\text{Laves\_C14}}_{\text{Ta:Ta}}$ – ${}^{0}G^{\text{Laves\_C14}}_{\text{Cr:Ta}}$	$(0.01 < T < 6000.0)$
${}^{0}L^{\text{Laves\_C14}}_{\text{Cr,Ta:}*}$	+158 832.7 – 30.0000 T	$(0.01 < T < 6000.0)$
${}^{0}L^{\text{Laves\_C14}}_{*\text{:Cr,Ta}}$	+35 574.3 – 30.0000 T	$(0.01 < T < 6000.0)$

[a] Gibbs energy in J/mol-formula; Temperature in Kelvin.

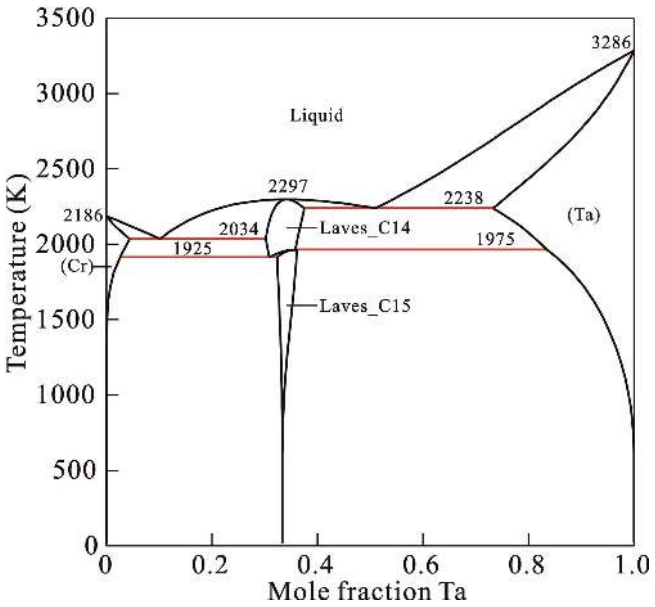

Fig. 4. Calculated Cr–Ta phase diagram down to 0 K according to the presently assessed thermodynamic parameters.

mental data from [23] in Fig. 3. As can be seen in Fig. 3, the presently calculated heat capacities are in excellent agreement with the experimental data over the wide temperature range. Moreover, an obvious improvement was achieved in comparison with the results in [13] because the present thermodynamic descriptions were extended to 0 K.

The optimization procedure of binary Cr–Ta system was executed by using the PARROT module incorporated in the Thermo-Calc software package [37] following the same assessment strategy used for the Co–Si system by Zhang et al. [38]. The entire optimization procedure could be separated into three steps. The optimization began with the intermetallic phases in the first step since its phase equilibria and thermodynamic information have been well-established, and both intermetallic phases, Laves_C15 and its high temperature modification Laves_C14 phase, were treated as stoichiometric compound Cr_2Ta. After that the parameters of BCC_A2 phase were derived by introducing the solubilities of Cr in (Ta) as well as Ta in (Cr). Then the phase equilibria information for two eutectics and the congruent melting point were taken into consideration to conduct the parameters for liquid phase. In the second step, the homogeneity range of Cr_2Ta phase was included and

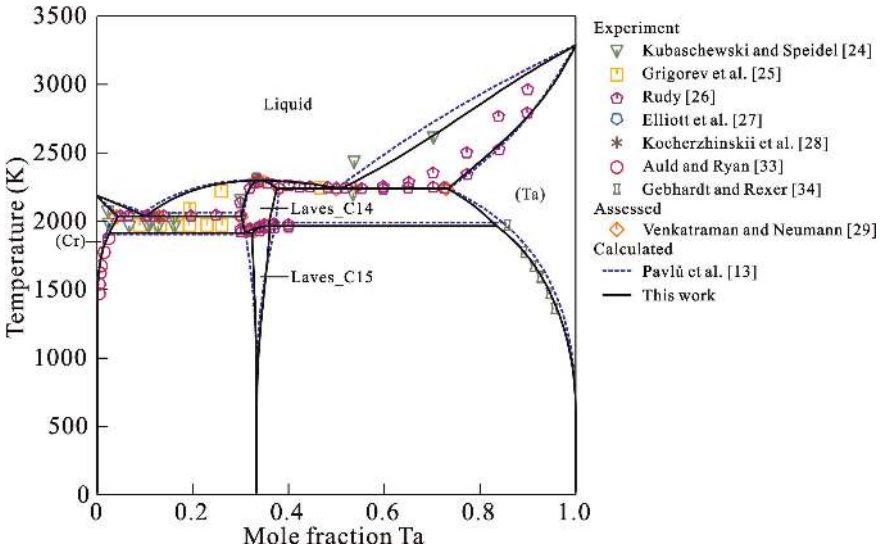

Fig. 5. Comparison between the calculated phase diagrams due to the thermodynamic descriptions from the present work and the previous assessment [13], compared with the experimental information [24–29, 33, 34] over the entire composition range.

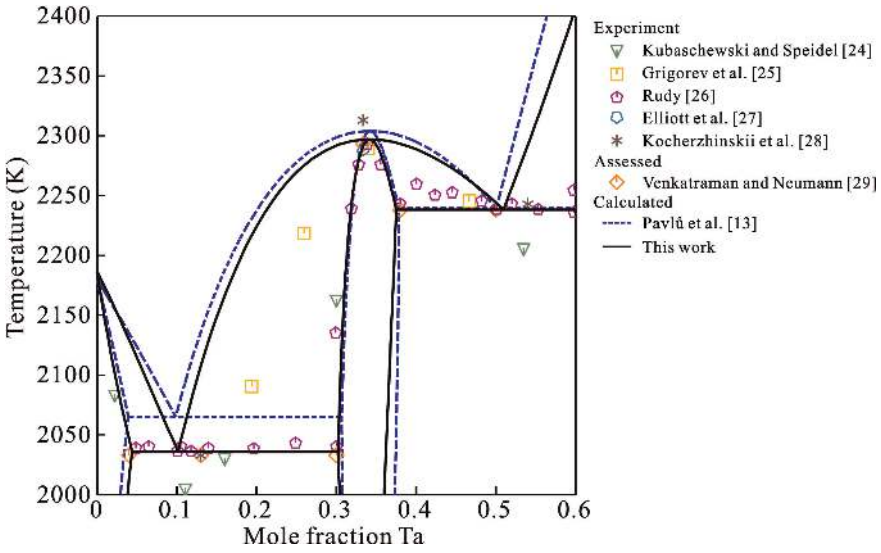

Fig. 6. Comparison between the calculated phase diagrams due to the thermodynamic descriptions from the present work and the previous assessment [13] and the experimental information [24–29] over the enlarged part around Laves_C14 phase.

the parameters of Cr_2Ta phase were thus derived. In the third step, the high temperature modification Laves_C14 phase was taken into account. The parameters obtained in the second step for Cr_2Ta phase were thought to be those of Laves_C15 phase. An equation of ${}^0G^{\text{Laves\_C14}}_{\text{Cr:Ta}} = {}^0G^{\text{Laves\_C15}}_{\text{Cr:Ta}} + A_0 + B_0 \cdot T$, as well as the eutectoid and the peritectoid were engaged into the optimization process of Laves_C14 phase. The finally obtained thermodynamic parameters are listed in Table 4.

The Cr–Ta phase diagram calculated over the entire composition range down to 0 K based on the thermodynamic parameters obtained in the present assessment is shown in Fig. 4. The comprehensive comparison between the calculated phase equilibria and the experimental information is presented in Fig. 5. Moreover, the calculated phase diagram in [13] is also appended in Fig. 5 for a direct comparison. As can been seen in Fig. 5, most of the experimental results can be well reproduced using the thermodynamic parame-

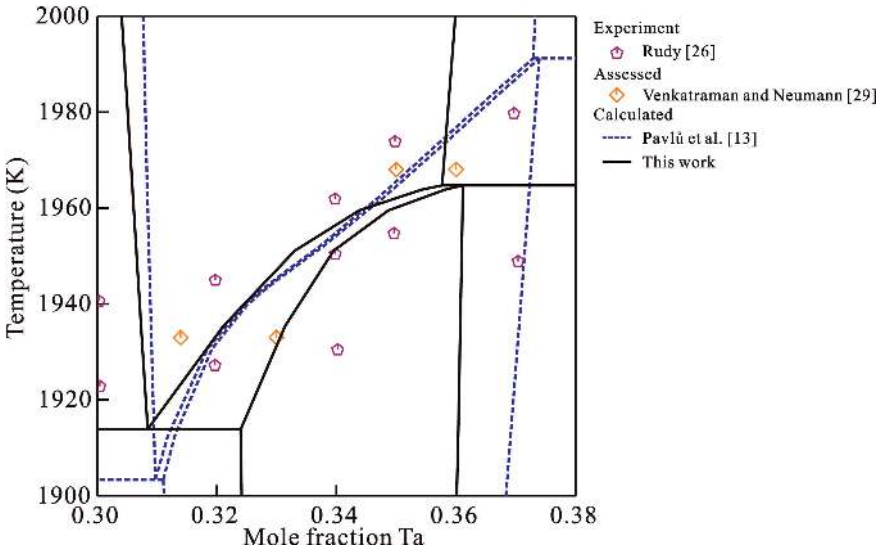

Fig. 7. Comparison between the calculated phase diagrams due to the thermodynamic descriptions from the present work and the previous assessment [13] and the experimental information [26, 29] over the enlarged part around the Laves_C14-Laves_C15 transformation.

Table 5. Summary of the invariant equilibria in the binary Cr–Ta system.

	Temperature (K)	Composition(at.%Ta)			Method	Reference
Congruent		L ↔ Laves_C14				
	2293 ± 20	33.3	33.3		Assessed	[29]
	2304	34.1	34.1		CALPHAD	[13]
	2297	34.2	34.2		CALPHAD	This work
Eutectic		L ↔ (Cr) + Laves_C14				
	2033 ± 20	~ 13.00	~ 4.00	~ 30.00	Assessed	[29]
	2040 ± 10	~ 10.50	~ 3.50	~ 30.00	Experiment	[26]
	–	9.60	–	–	Experiment	[6]
	2065	9.88	3.91	30.65	CALPHAD	[13]
	2036	10.18	4.40	30.23	CALPHAD	This work
Eutectic		L ↔ (Ta) + Laves_C14				
	2238 ± 20	~ 50.00	~ 73.00	~ 38.00	Assessed	[29]
	2239	50.03	73.41	37.84	CALPHAD	[13]
	2238	50.94	73.29	37.50	CALPHAD	This work
Eutectoid		Laves_C14 ↔ (Cr) + Laves_C15				
	1933	~ 31.40	–	~ 33.00	Assessed	[29]
	1903	30.97	1.87	31.11	CALPHAD	[13]
	1914	30.85	2.64	32.40	CALPHAD	This work
Peritectoid		Laves_C14 + (Ta) ↔ Laves_C15				
	1968	~ 35.00	–	~ 36.00	Assessed	[29]
	1991	37.29	84.71	37.39	CALPHAD	[13]
	1963	35.76	83.50	36.03	CALPHAD	This work

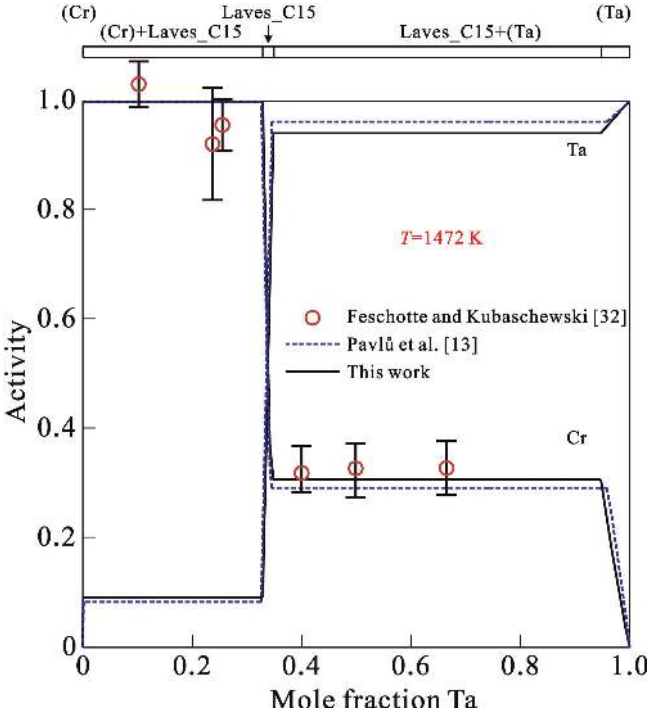

Fig. 8. Calculated activities of Cr and Ta at 1 472 K, compared to the calculated results by Pavlů et al. [13] and the experimental data from [32].

Table 6. List of enthalpy of formation of Laves_C15 Cr_2Ta compound at different temperatures from the literature and the present work.

Temperature (K)	ΔH_f (J/mol-atom)	Method	Reference
0	–11 290	Ab initio	[13]
	–8 939	CALPHAD	This work
298	–11 283	CALPHAD	[13]
	–8 926	CALPHAD	This work
1 673	–8 521 ± 500	Experiment	[32]
	–10 635	CALPHAD	[13]
	–8 104	CALPHAD	This work

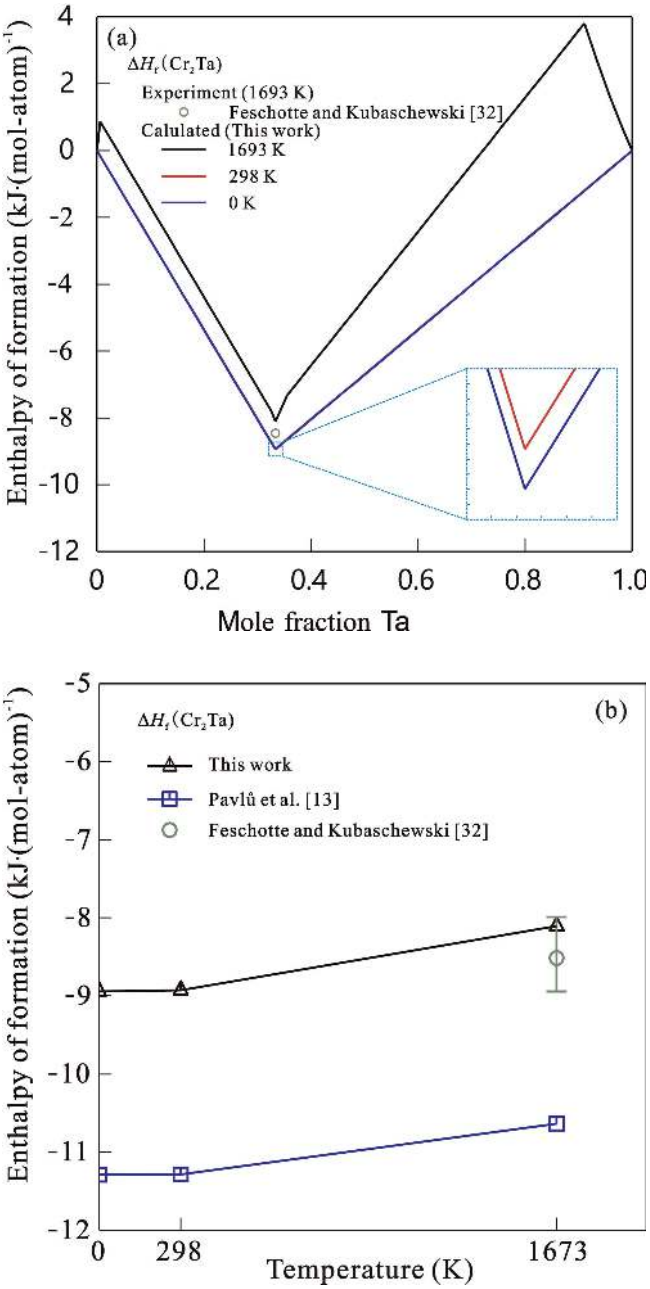

Fig. 9. (a) Calculated enthalpy of formation of Cr2Ta compound at different temperatures over the entire composition range in comparison with the experimental data from [32]; (b) Calculated enthalpy of formation of Cr2Ta compound at different temperatures, compared to the calculated results by Pavlů et al. [13], and the experimental data from [32].

ters obtained in the present work as well as previous assessment [13]. Furthermore, the present work achieves a better agreement with the Ta solvus determined by Gebhardt and Rexer [34]. The calculated temperatures of liquidus in the Ta rich part by the present work are lower than those in the previous assessment [13], but agree well with the experimental results [26].

The enlarged part of phase equilibria around congruent melting points and two eutectics of Fig. 5 is presented in Fig. 6, while the enlargement for the phase equilibria around eutectoid and peritectoid in Fig. 5 is presented in Fig. 7, both are in comparison with the existing experimental results as well as the calculated phase diagram in the previous assessment [13]. The calculated/experimental invariant equilibria are listed in Table 5. As can be seen from Fig. 6 and Fig. 7, the calculated phase equilibria in the vicinity of Laves_C15 and Laves_C14 phases show better agreement with the experimental data [26] than the calculated results according to the previous assessment by Pavlů et al. [13]. This fact indicates that the noticeable improvement is achieved in the present assessments, in comparison with the previous one [13].

Figure 8 presents the calculated activities of Cr and Ta over the entire composition range at 1472 K, compared with the experimental data over the two-phase regions of (Cr) + Laves_C15 and (Ta) + Laves_C15 [32] as well as the calculated results [13]. As can be seen, the calculated

activities are always within the uncertainties of the experimental data. Moreover, the calculated results due to the present work and the previous assessments [13] also agree with each other.

Nowadays, the coupling between the first-principles calculations and CALPHAD becomes the standard way to remedy the missing experimental information such as the case study of re-modeling of Cr–Ta by Pavlů et al. [13]. However, it should be noted that the enthalpies computed using first-principles calculations at 0 K are usually utilized as standard enthalpies of formation at 298 K in the CALPHAD-type thermodynamic assessment, as done in [13]. Actually, such treatment unavoidably ignores the difference of enthalpies of formation between 0 K and 298 K. What's more, for some cases such as the binary system Cr–Nb, the first-principles calculations from different sources are inconsistent with each other [22]. Thus, the measured enthalpy of formation of Cr_2Ta at 1673 K [32] was employed in the present thermodynamic assessment, while the calculated enthalpy of formation of Cr_2Ta in [13] was just used for comparison. The calculated enthalpies of formation of Cr_2Ta at various temperatures are listed in Table 6 and presented in Fig. 9, compared with the calculated results by Pavlů et al. [13]. The experimental result by Feschotte and Kubaschewski [32] is also appended for comparison. As can be seen in Fig. 9b, the calculated enthalpy of formation of Cr_2Ta at 1673 K obtained in the present work is within the experimental uncertainties, while for the calculated results derived from Pavlů et al. [13] shows a large deviation from the experimental data. In fact, as indicated in Fig. 9b, the calculated enthalpies of formation of Cr_2Ta in the present work show a large discrepancy in comparison with the results derived from Pavlů et al. [13].

5. Conclusion

A thermodynamic re-assessment of the binary Cr–Ta system down to 0 K based on the new description of the Gibbs energy for pure elements was performed using the CALPHAD technique. The experimental information ignored in the previous assessments, including the low-temperature heat capacities of Cr_2Ta and the newly emerging phase equilibria information on Cr-rich part eutectic, were taken into account. The obtained thermodynamic descriptions for the binary Cr–Ta system were finally validated by comprehensively comparing the calculated phase equilibria and thermodynamic properties with the experimental data and the previous CALPHAD assessments. Noticeable improvement was achieved in the present thermodynamic assessment, in comparison with the previous assessments.

The financial support from the Hunan Provincial Science and Technology Program of China (Grant No. 2017RS3002) – Huxiang Youth Talent Plan and the Youth Talent Project of Innovation-driven Plan at Central South University (2019CX027), the Collabtrative Research Center "Superalloys Single Crystal" (TR-103 project C6) of the German Research Foundation (DFG) and the Sino-German Cooperation Project GZ1208 is acknowledged.

References

[1] M. Brady, J. Zhu, C. Liu, P. Tortorelli, L. Walker, C. McKamey, J. Wright, C. Carmichael, D. Larson, M. Miller, W. Porter: Mater. High Temp. 16 (1999) 189. DOI:10.1179/mht.1999.018
[2] M. Brady, J. Zhu, C. Liu, P. Tortorelli, L. Walker: Intermetallics 8 (2000) 1111. DOI:10.1016/S0966-9795(00)00046-7
[3] K. Kumar, L. Pang, C. Liu, J. Horton, E. Kenik: Acta Mater. 48 (2000) 911. DOI:10.1016/S1359-6454(99)00377-8
[4] Y. Ro, Y. Koizumi, S. Nakazawa, T. Kobayashi, E. Bannai, H. Harada: Scr. Mater. 46 (2002) 331. DOI:10.1016/S1359-6462(01)01244-1
[5] Y. Gu, H. Harada, Y. Ro: JOM. 56 (2004) 28. DOI:10.1007/s11837-004-0197-0
[6] A. Bhowmik, H. Stone: Metall. Mater. Trans. A 43 (2012) 3283. DOI:10.1007/s11661-012-1140-6
[7] V. Choda, A. Bhowmik, I. Edmonds, C. Jones, H. Stone: MRS Online Proc. Libr. 1516 (2013) 275–281. DOI:10.1557/opl.2013.142
[8] A. Luo: CALPHAD: Comput. Coupling Phase Diagrams Thermochem. 50 (2015) 6. DOI:10.1016/j.calphad.2015.04.002
[9] Z. Lu, L. Zhang: Mater. Des. 116 (2017) 427. DOI:10.1016/j.matdes.2016.12.034
[10] L. Kaufman: CALPHAD: Comput. Coupling Phase Diagrams Thermochem. 15 (1991) 243. DOI:10.1016/0364-5916(91)90004-4
[11] N. Dupin, I. Ansara: J. Phase Equilib. 14 (1993) 451. DOI:10.1007/BF02671963
[12] F. Zhang, S. Chen, Y. Chang, W. Oates: Intermetallics 9 (2001) 1079. DOI:10.1016/S0966-9795(01)00101-7
[13] J. Pavlů, J. Vřešťál, M. Šob: CALPHAD: Comput. Coupling Phase Diagrams Thermochem. 33 (2009) 179. DOI:10.1016/j.calphad.2008.04.006
[14] M. Chase, I. Ansara, A. Dinsdale, G. Eriksson, G. Grimvall, L. Hoglund, H. Yokokawa: CALPHAD: Comput. Coupling Phase Diagrams Thermochem. 19 (1995) 437. DOI:10.1016/0364-5916(96)00002-8
[15] Q. Chen, B. Sundman: J. Phase Equilib. 22 (2001) 631. DOI:10.1007/s11669-001-0027-9
[16] M. Palumbo, B. Burton, A. Costa e Silva, B. Fultz, B. Grabowski, G. Grimvall, B. Hallstedt, O. Hellman, B. Lindahl, A. Schneider, P.E.A. Turchi, W. Xiong: Phys. Status Solidi B 251 (2014) 14. DOI:10.1002/pssb.201350133
[17] W. Xiong, P. Hedström, M. Selleby, J. Odqvist, M. Thuvander, Q. Chen: CALPHAD: Comput. Coupling Phase Diagrams Thermochem. 35 (2011) 355. DOI:10.1016/j.calphad.2011.05.002
[18] S. Bigdeli, H. Mao, M. Selleby: Phys. Status Solidi B 252 (2015) 2199. DOI:10.1002/pssb.201552203
[19] Y. Tang, L. Zhang: Materials 11 (2018) 1648. PMid:30142900; DOI:10.3390/ma11091648
[20] I. Roslyakova, B. Sundman, H. Dette, L. Zhang, I. Steinbach: CALPHAD: Comput. Coupling Phase Diagrams Thermochem. 55 (2016) 165. DOI:10.1016/j.calphad.2016.09.001
[21] I. Roslyakova, S. Zomorodpoosh, R. Otis, L. Zhang, I. Steinbach: New generation CALPHAD databases: accurate approximation of the Debye model based on segmented regression and linear combination of Einstein functions (Poster, CALPHAD Conference 2017 in Saint Malo, France) (2017).
[22] Y. Jiang, S. Zomorodpoosh, I. Roslyakova, L. Zhang: CALPHAD: Comput. Coupling Phase Diagrams Thermochem. 62 (2018) 109. DOI:10.1016/j.calphad.2018.06.001
[23] J.F. Martin, F. Müller, O. Kubaschewski: Trans. Faraday Soc. 66 (1970) 1065. DOI:10.1039/TF9706601065
[24] O. Kubaschewski, H. Speidel: J. Inst. Metals 16 (1949).
[25] A. Grigorev, V. Kuprina, N. Nedumov: Russ. J. Inorg. Chem. 4 (1959) 296.
[26] E. Rudy: Ternary phase equilibria in transition metal-boron-carbon-silicon systems. part 5. compendium of phase diagram data. Tech. rep., AEROJET-GENERAL CORP SACRAMENTO CA MATERIALS RESEARCH LAB (1969).

[27] R. Elliott, W. Rostoker: Trans. ASM 50 (1958) 617.
[28] Y. Kocherzhinskii, V. Petkov, E. Shishkin: Phase equilibrium and crystal structure of the intermediate phase in the Ta–Cr system. Tech. rep., Inst. of Metal Physics, Kiev (1973).
[29] M. Venkatraman, J. Neumann: J. Phase Equilib. 8 (1987) 112. DOI:10.1007/BF02873190
[30] D. Wang, P. Liaw, C. Liu, E. George: Processing and microstructures of Cr–Ta and Cr–Ta–Mo Composites Reinforced by the Cr_2Ta laves phase. Tech. rep., The University of Tennessee, Knoxville, TN (US); Oak Ridge National Lab., Oak Ridge, TN (US) (2003). DOI:10.2172/814616
[31] P. Duwez, H. Martens: JOM 4 (1952) 72. DOI:10.1007/BF03397652
[32] P. Feschotte, O. Kubaschewski: Trans. Faraday Soc. 60 (1964) 1941. DOI:10.1039/TF9646001941
[33] J. Auld, N. Ryan: J. Less-Common Met. 3 (1961) 221. DOI:10.1016/0022-5088(61)90063-7
[34] E. Gebhardt, J. Rexer: PRECIPITATIONS IN Ta–Cr solid solutions. Tech. rep., Max-Planck-Institut fuer Metallforschung, Stuttgart (1967).
[35] O. Redlich, A. Kister: Ind. Eng. Chem. Res. 40 (1948) 345. DOI:10.1021/ie50458a036
[36] M. Hillert, M. Jarl: CALPHAD: Comput. Coupling Phase Diagrams Thermochem. 2 (1978) 227. DOI:10.1016/0364-5916(78)90011-1
[37] B. Sundman, B. Jansson, J. Andersson: CALPHAD: Comput. Coupling Phase Diagrams Thermochem. 9 (1985) 153. DOI:10.1016/0364-5916(85)90021-5
[38] L. Zhang, Y. Du, H. Xu, Z. Pan: CALPHAD: Comput. Coupling Phase Diagrams Thermochem. 30 (2006) 470. DOI:10.1016/j.calphad.2006.06.001
[39] F. Simon, C. Simson, M. Ruhernann: Z. Phys. Chem. 129 (1927) 339. DOI:10.1002/zaac.19271680121
[40] F. Jaeger, E. Rosenbohm: Recl. Trav. Chim. Pays-Bas. 53 (1934) 451. DOI:10.1002/recl.19340530511
[41] C. Anderson: J. Am. Chem. Soc. 59 (1937) 488. DOI:10.1021/ja01282a018
[42] L. Armstrong, H. Grayson-Smith: Can. J. Res. 28 (1950) 51. DOI:10.1139/cjr50a-004
[43] I. Estermann, S. Friedberg, J. Goldman: Phys. Rev. 87 (1952) 582. DOI:10.1103/PhysRev.87.582
[44] J. Rayne, W. Kemp: Philos. Mag. 1 (1956) 918. DOI:10.1080/14786435608238169
[45] F. Krauss: Z. Metallkd. 49 (1958) 386.
[46] H. Martin: Ph. D. thesis, Univ. of Koeln (1958).
[47] R. Beaumont, H. Chihara, J. Morrison: Philos. Mag. 5 (1960) 188. DOI:10.1080/14786436008243302
[48] K. Clusius, P. Franzosini: Z. Naturforschg. 17A (1962) 522. DOI:10.1515/zna-1962-0611
[49] G. Kalishevich, P. Geld, R. Krentsis: Zh. Fiz. Khim. 39 (1965) 2999.
[50] R. Kohlhaas, M. Braun, O. Vollmer: Z. Naturforsch. A: Phys. Sci. 20 (1965) 1077. DOI:10.1515/zna-1965–0814
[51] T. Kemeny, B. Fogarassy, S. Arajs, C. Moyer: Phys. Rev. B. 19 (1979) 2975. DOI:10.1103/PhysRevB.19.2975
[52] A. Magnus, H. Holzmann: Ann. Phys. 395 (1929) 585. DOI:10.1002/andp.19293950504
[53] F. Jaeger, W. Veenstra: Recl. Trav. Chim. Pays-Bas. 53 (1934) 677. DOI:10.1002/recl.19340530802
[54] W. Keeson, M. Desirant: Physica. 8 (1941) 273. DOI:10.1016/S0031-8914(41)90048-4
[55] K. Clusjus, C. Losa: Z. Naturforsch. A: Phys. Sci. 10 (1955) 939. DOI:10.1515/zna-1955-1207
[56] K. Sterrett, W. Wallace: J. Am. Chem. Soc. 80 (1958) 3176. DOI:10.1021/ja01546a002
[57] D. White, C. Chou, H. Johnston: Phys. Rev. 109 (1958) 797. DOI:10.1103/PhysRev.109.437
[58] G. Lehman: Thermal properties of refractory materials. Tech. rep., Atomics International. Div. of North American Aviation, Inc., Canoga Park, Calif. (1960).
[59] M. Hoch, H. Johnston: J. Phys. Chem. 65 (1961) 855. DOI:10.1021/j100823a033
[60] G. Lowenthal: Aust. J. Phys. 16 (1963) 47. DOI:10.1071/ph630047
[61] R. Taylor, R. Finch: J. Less-Common Met. 6 (1964) 283. DOI:10.1016/0022-5088(64)90124-9

(Received January 10, 2019; accepted March 23, 2019; online since July 10, 2019)

Correspondence address

Dr. Irina Roslyakova
ICAMS
Ruhr-Universität Bochum
Universitätsstr. 150
Bochum 44801
Germany
Tel.: +49 234 32 22605
Fax: +49 234 32 14989
E-mail: irina.roslyakova@rub.de

Professor Dr. Lijun Zhang
State Key Lab of Powder Metallurgy
Central South University
Changsha, Hunan, 410083
P. R. China
Tel.: +86-731-88836812
Fax: +86-731-88710855
E-mail: xueyun168@gmail.com
lijun.zhang@csu.edu.cn

Bibliography
DOI 10.3139/146.111812
Int. J. Mater. Res. (formerly Z. Metallkd.)
110 (2019) 9; page 797 – 807

ISSN 1862-5282